Adaptive aberration compensation for three-dimensional micro-fabrication of photonic crystals in lithium niobate

Benjamin P. Cumming,[1] **Alexander Jesacher,**[2] **Martin J. Booth,**[3,4]
Tony Wilson,[3] **and Min Gu**[1,*]

[1]*Centre for Micro-Photonics and CUDOS, Faculty of Engineering and Industrial Sciences, Swinburne University of Technology, Hawthorn, Victoria 3122, Australia*
[2]*Division of Biomedical Physics, Innsbruck Medical University, Müllerstr. 44, A-6020 Innsbruck, Austria*
[3]*Department of Engineering Science, University of Oxford, Parks Road, Oxford, OX1 3PJ, UK*
[4]*martin.booth@eng.ox.ac.uk*

[*]mgu@swin.edu.au

Abstract: We present the use of a liquid crystal spatial light modulator to correct for the refractive-index mismatch induced spherical aberration in a high refractive-index lithium niobate crystal when a low repetition rate amplified laser is used for the direct fabrication of three-dimensional micro-structures. By correcting the aberration based on experimentally determined values, we show that the size of written structures decreases dramatically, which allows the fabrication of high quality micro-structures such as three-dimensional photonic crystals. We demonstrate that, through the use of adaptive optics, the fabrication depth and the stopgap strength in the corresponding photonic crystals are increased by a factor of two to three.

© 2011 Optical Society of America

OCIS codes: (220.1080) Active or adaptive optics; (220.1000) Aberration compensation; (220.4000) Microstructure fabrication; (160.5298) Photonic crystals; (160.3730) Lithium niobate.

References and links

1. P. Török, P. Varga, Z. Laczik, and G. R. Booker, "Electromagnetic diffraction of light focused through a planar interface between materials of mismatched refractive indices: an integral representation," J. Opt. Soc. Am. B **12,** 325–332 (1995).
2. M. Gu, *Advanced Optical Imaging Theory* (Springer, 1999).
3. G. Zhou and M. Gu, "Anisotropic properties of ultrafast laser-driven microexplosions in lithium niobate crystal," Appl. Phys. Lett. **87,** 241107 (2005).
4. G. Zhou, A. Jesacher, M. Booth, T. Wilson, A. Ródenas, D. Jaque, and M. Gu, "Axial birefringence induced focus splitting in lithium niobate," Opt. Express **17,** 17970–17975 (2009).
5. S. Wong, M. Deubel, F. Prez-Willard, S. John, G. A. Ozin, M. Wegener, and G. von Freymann, "Direct laser writing of three-dimensional photonic crystals with a complete photonic bandgap in chalcogenide glasses," Adv. Mater. **18,** 265–269 (2006).
6. D. Day and M. Gu, "Effects of refractive-index mismatch on three-dimensional optical data-storage density in a two-photon bleaching polymer," Appl. Opt. **37,** 6299–6304 (1998).
7. M. Booth, M. Schwertner, T. Wilson, M. Nakano, Y. Kawata, M. Nakabayashi, and S. Miyata, "Predictive aberration correction for multilayer optical data storage," Appl. Phys. Lett. **88,** 031109 (2006).
8. C. Mauclair, A. Mermillod-Blondin, N. Huot, E. Audouard, and R. Stoian, "Ultrafast laser writing of homogeneous longitudinal waveguides in glasses using dynamic wavefront correction," Opt. Express **16,** 5481–5492 (2008).
9. A. Jesacher, G. D. Marshall, T. Wilson, and M. J. Booth, "Adaptive optics for direct laser writing with plasma emission aberration sensing," Opt. Express **18,** 656–661 (2010).

10. G. Zhou and M. Gu, "Direct optical fabrication of three-dimensional photonic crystals in a high refractive index LiNbO3 crystal," Opt. Lett. **31,** 2783–2785 (2006).
11. A. Ródenas, G. Zhou, D. Jaque, and M. Gu, "Rare-earth spontaneous emission control in three-dimensional lithium niobate photonic crystals," Adv. Mater. **21,** 3526–3530 (2009).
12. A. Jesacher and M. J. Booth, "Parallel direct laser writing in three dimensions with spatially dependent aberration correction," Opt. Express **18,** 21090–21099 (2010).
13. S. Stallinga, "Light distribution close to focus in biaxially birefringent media," J. Opt. Soc. Am. A **21,** 1785–1798 (2004).

1. Introduction

When a focused wavefront converges through a planar refractive-index mismatch interface, strong spherical aberration is imparted onto the beam, which distorts the focal energy distribution [1, 2]. This poses a problem for fabrication of three-dimensional (3D) micro-structures with direct laser writing (DLW) where small and symmetric focal shapes are often desired. The problem is particularly pronounced when a high numerical aperture (NA) objective is used for fabrication in high refractive index materials such as lithium niobate ($LiNbO_3$) [3, 4] where the refractive index of the crystal ($n \approx 2.2$ at wavelength 790 nm) is significantly different to that of the typical objective immersion oil ($n \approx 1.5$). Under these conditions, the spherical aberration is severe and causes significant defocus, focal elongation and distortion together with a corresponding reduction in peak intensity. Furthermore, the aberration increases in proportion to the fabrication depth and hence hinders high resolution, symmetric and consistent fabrication over a large volume of material.

Although there have been several reports regarding compensation for the spherical aberration [5–9], only three attempts have recently been developed to overcome this challenging and more pronounced problem in $LiNbO_3$. The first is to fabricate micro-voids in $LiNbO_3$ through DLW in terms of the so-called threshold method with a high repetition rate laser (82 MHz) [10]. Though the elongation of the focal spot within a $LiNbO_3$ film can be partially reduced by lowering the fabrication laser power to a level that is slightly above the threshold of the micro-explosion in $LiNbO_3$, no spherical aberration is compensated for in this process. As such, only quasi-spherical voids can be generated within a limited fabrication depth [10]. In addition, a high repetition rate laser can also cause the accumulative heating effect that may degrade the quality of voids. Both the fabrication depth and the heating effect have been addressed by the use of a low repetition rate laser amplifier (1 kHz) in combination of the threshold method [11]. However, significant cracks can be induced by an amplified and aberrated pulsed laser beam [11]. Direct compensation for the spherical aberration in $LiNbO_3$ has been demonstrated by the use of a liquid crystal spatial light modulator (SLM) to perform adaptive aberration correction for fabrication [12]. Unfortunately, the reported method is based on the generation of multiple focal spots with aberration compensation. While the generation of multiple focal spots is useful for increasing the speed of fabrication, the technique has failed to generate a series of well-arranged periodic arrays due to the inherent off-axis chromatic aberration that limits the uniformity of the multiple focal spots. Thus, the fabrication of 3D well-arranged periodic microstructures such as 3D photonic crystals (PhCs) with stopgaps was impossible [12]. In this paper, we present the first demonstration of adaptive spherical aberration compensation for 3D micro-fabrication of functional PhCs in $LiNbO_3$.

2. Theoretical analysis

The origin of the refractive-index mismatch aberration is an optical path length difference between rays traveling through the interface at different angles of convergence. Each angle traverses through a different ratio of the two materials which results in differing phase delays. The

aberration is well understood and can be represented in the case of a planar interface between isotropic immersion (n_1) and fabrication (n_2) refractive indices by [1,2]:

$$\psi = kd(n_2 \cos\theta_2 - n_1 \cos\theta_1) \tag{1}$$

where θ_1 and θ_2 are the angles of convergence in the immersion and fabrication medium respectively and d is the nominal focusing depth as shown in the experimental setup. The factor k is the wavenumber given by $2\pi/\lambda$ where λ is the wavelength in vacuum. The function contains both defocus and spherical aberration terms that shift and distort the focal point respectively.

In addition to this, the uniaxial birefringence of LiNbO$_3$ causes other aberration effects [13]. To minimize these aberrations, it is necessary to orient the crystal so that the principal axis is perpendicular to the optical axis and to use linearly polarized illumination aligned to the predominately linear ordinary polarization eigenmode. This ensures that the additional aberration primarily consists of defocus and spherical aberration. Other crystal orientations and polarizations lead to more complex aberrations [3,4]. For LiNbO$_3$, we can achieve this alignment with either an X- or Y-cut crystal. Figure 1(a) shows the focal intensity distribution when a plane wave is focused into a nominal depth of 0 μm, 7.5 μm and 20 μm in a LiNbO$_3$ slab without compensation for the refractive-index mismatch aberration. Figure 1(b) shows plots along the axial direction of the three depths in Fig. 1(a). The NA in the calculation was set at 1.4 with an immersion medium of refractive index 1.52 and LiNbO$_3$ ordinary and extraordinary indices of 2.18 and 2.26 for a wavelength of 790 nm. It is clear that the refractive-index mismatch causes severe defocus, distortion and intensity drop that increases in severity with depth. Figure 1(c) shows plots along the axial direction when the refractive-index mismatch aberration is compensated with the isotropic aberration function in Eq. (1) using the average of the ordinary and extraordinary refractive indices for n_2. The effect of aberration is almost entirely reduced and the focal intensity distribution restored close to the diffraction limit at each depth.
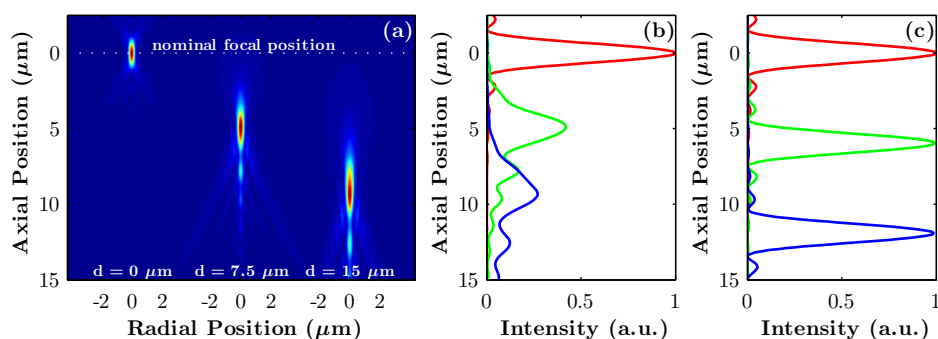
Fig. 1. (a) Calculated focal intensity distribution when a plane wave is focused into depths of 0 μm, 7.5 μm and 15 μm in LiNbO$_3$ without compensation of the refractive-index mismatch aberration. (b) Comparison of the intensity along the axial direction in (a). (c) Intensity along the axial direction in (a) when the aberration is compensated.

3. Experimental aberration compensation

To achieve compensation of the refractive-index mismatch aberration experimentally it is necessary to alter the phase of the wavefront entering the objective. This can be realized accurately for moderate strength aberrations through the addition of a liquid crystal based SLM into the beam path that pre-aberrates the beam with the conjugate of the refractive-index mismatch aberration. We implemented this by introducing a liquid crystal based SLM (Hamamatsu X10468-02) into a DLW system, as pictured in Fig. 2. The laser was an amplified Ti-sapphire system

(Newport Spectra Physics Solstice) operating at a wavelength of 790 nm, a pulse width of 100 fs and a repetition rate of 1 kHz. The objective was an Olympus PlanApo (60x, 1.4 NA). Computer control of the SLM, laser and 3D translation stage allows for compensation of aberration at all points of fabrication.

To aid the SLM's ability to replicate large aberrations, we corrected for the defocus by positioning the objective at a nominal focal depth that would refract to the desired fabrication location. This left only the weaker spherical aberration ($\approx 20\%$ of total magnitude) components to be compensated by the SLM, allowing for accurate performance over a larger range of depths. Furthermore, in the case of $LiNbO_3$ where $n_2 > n_1$, refraction shifts the focus away from the surface. The nominal focus depth will therefore be less than the desired depth of fabrication, reducing the amount of spherical aberration to be compensated. Figure 3(a) shows the phase patterns displayed on the SLM for a depth of 20 μm with (top) and without (bottom) the inclusion of the defocus. The transition between black and white corresponds to a phase wrapping between 0 to 2π. It is clear that removing the defocus greatly reduces the complexity of the correction pattern.
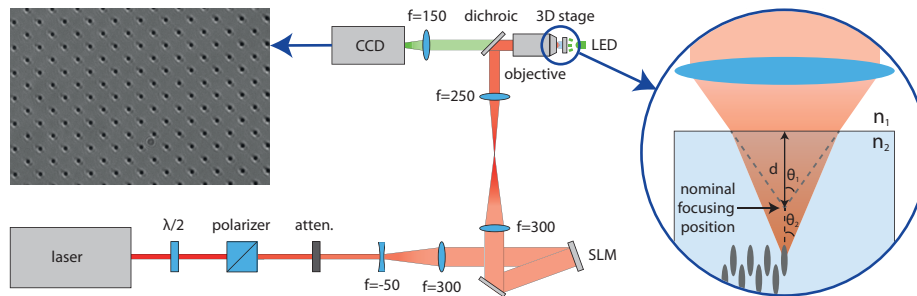
Fig. 2. Experimental set-up used for DLW with a SLM. The insets show a typical image of a plane in a fabricated PhC (left) and the focusing conditions within the fabrication medium when $n_2 > n_1$ (right).

Once each nominal focal depth was determined, a basic adaptive method was utilized to ensure the SLM was correcting for the optimum amount of aberration at that depth. This involved adjustment of the fabrication pulse energy and the scale of the aberration correction whilst monitoring the sample for presence of fabrication. Only when the correction was at an optimum level was the peak focal intensity greatest, thus requiring the lowest fabrication pulse energy to reach the fabrication threshold.
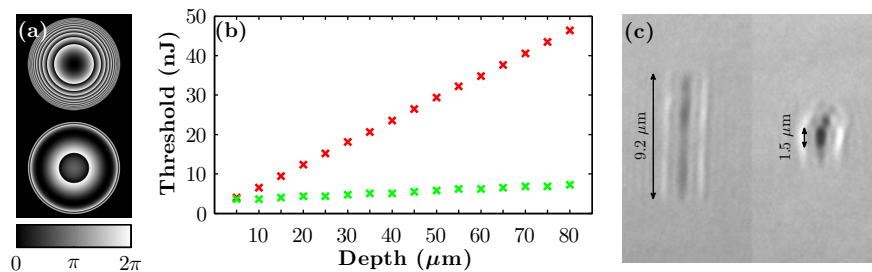
Fig. 3. (a) Phase pattern displayed on the SLM with (top) and without (bottom) inclusion of the defocus. (b) Plot of the measured fabrication threshold energy for the uncompensated (red) and compensated (green) cases. (c) Side views of fabricated voxels at a depth of 20 μm when the beam is uncompensated (left) and compensated (right).

4. Aberration corrected fabrication of photonic crystals

The resulting fabrication thresholds for both the uncompensated and compensated beams can be seen in Fig. 3(b). A large increase in energy is required to fabricate at larger depths with an uncompensated beam due to the drop in peak focal intensity with depth, while only a small increase in energy is needed when aberration compensation is employed. The increase required when aberration compensation is employed is due to a combination of a small amount of birefringence induced aberration as well as a drop in the SLM accuracy and efficiency when replicating aberrations with large gradient and amplitude.

To confirm the effectiveness of the aberration correction, a LiNbO$_3$ crystal with polished sides was used to fabricate single regions of modified material, hereafter termed 'voxels', at a depth of 20 μm and close to the crystal edge so that a side view of the fabricated region could be observed by rotating the crystal by 90 degrees. The fabrication was performed with the crystal principal axis perpendicular to the optical axis (Y-cut) and imaging performed with the principal axis parallel to the optical axis (Z-cut). Although the focal splitting phenomenon associated with the Z-cut crystal [4] affects imaging performance, the images [Fig. 3(c)] clearly show the effects of aberrations on voxel shape. When the beam is uncompensated, the axial length of the voxel was observed to be 9.2 μm when a pulse energy of 54 nJ and an exposure time of 50 ms was employed. When we applied the optimal level of aberration compensation needed at that depth, the size of the focal spot decreased dramatically to 1.5 μm indicating greatly reduced aberration.
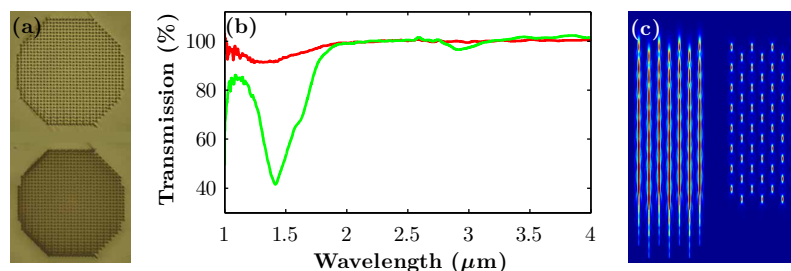
Fig. 4. (a) Transmission microscope images of the top view of FCC PhCs of 50 layers and of lattice constant 4.5 μm fabricated without (top) and with (bottom) compensation of the refractive-index mismatch aberration. (b) Smoothed transmission spectrum of the uncompensated (red) and compensated (green) PhCs in (a). (c) Calculated focal intensity distributions that occur when fabricating the top 16 layers of the uncompensated (left) and compensated (right) PhCs in (a).

This improved voxel shape was then utilized to fabricate more complex micro-structures with much higher quality. As an example, we arranged the voxels into a face centered cubic (FCC) 3D PhC structure with a lattice constant of 4.5 μm. The top layer was positioned 8 μm below the surface of the crystal and 50 layers were fabricated to a maximum depth of 118 μm. PhCs were fabricated both with and without compensation of the refractive-index mismatch aberration, and the transmission spectrum of the PhCs measured using a Fourier transform infrared spectrometer (Thermo Nicolet, Madison, Wis). Top views of the corrected and uncorrected PhCs are shown in Fig. 4(a) alongside their corresponding transmission spectrum in Fig. 4(b). A very clear transmission suppression was observed for the compensated PhC (green), blocking 60 % of incident light at a wavelength of 1.4 μm along with a slight suppression at the 2.8 μm wavelength position. These stopgap positions agree well with previously fabricated FCC PhCs in LiNbO$_3$ and show a three-fold improvement in suppression over previously obtainable results using a low repetition rate laser [11]. Furthermore, it can be seen that the maximum

fabrication depth is increased by a factor of 2.5 in comparison with the previous result [11]. For the uncorrected case (red) only a slight suppression is seen around the 1.4 μm position with no suppression at 2.8 μm. The reduction in strength can be attributed to aberrated focal points at large depths having a complex and elongated shape that merge into those vertically adjacent, forming an almost continuous structure in the direction of the incident beam that does not contribute to the stopgap. This is depicted by the calculated focal intensity distributions in Fig. 4(c) that occur when fabricating the first 16 layers of the PhCs. The individual focal intensity distributions merge into each other when uncompensated (left) but remain separated when compensated (right). At larger depths, the aberration and hence merging of layers is more pronounced while the compensated focal distributions remain separated. The limit on the depth of fabrication is ultimately determined by the resolution of the SLM. At large depths, the limited number of pixels available will no longer be able to replicate the required aberration function and the quality of correction and fabrication will decline.

To determine the level of improvement gained with an adaptive compensation scheme, we fabricated PhCs by both the adaptive method and with correction limited to the value provided by the isotropic aberration function in Eq. (1). Consequently, an uncompensated beam results in the weakest stopgaps, while compensating at the theoretically predicted level improves the suppression but the improvement is still smaller than that seen when the measured aberration is used for compensation [Figs. 5(a)–5(d)]. This indicates that an adaptive measurement and correction system must be utilized if the best quality fabrication is to be achieved. Finally, we fabricated PhCs at increasingly larger depths to demonstrate that quality can be maintained over a larger volume of material. Figures 5(a)–5(d) show the PhC transmission spectrum for four different PhCs fabricated at different depths below the surface. The energy used to fabricate at each depth was increased to the maximum level above the fabrication threshold of the adaptively compensated PhC before a stress induced crack formed across the PhC. As the depth is increased, the uncompensated PhCs lose their stopgaps while the compensated PhCs increase their stopgap strength despite the increase in aberration at larger depths. This is the result of compensation of the refractive-index mismatch maintaining the quality of the PhC structure over a larger range of depths such that the increase in fabrication energy can produce stronger stopgaps.
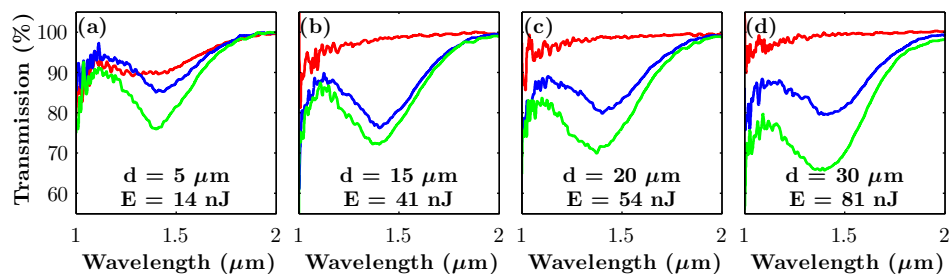
Fig. 5. Smoothed transmission spectrum of FCC PhCs of 16 layers and a lattice constant of 4.5 μm fabricated with a depth below the surface and energy above fabrication threshold of (a) 5 μm and 14 nJ, (b) 15 μm and 41 nJ, (c) 20 μm and 54 nJ, (d) 30 μm and 81 nJ. The red spectrum correspond to PhCs with no compensation while the blue and green spectrum correspond to PhCs with aberration compensation based on the isotropic aberration function and our adaptive compensation method, respectively.

5. Conclusion

We have applied liquid crystal SLM based adaptive optics to the fabrication of 3D PhCs in a high refractive-index $LiNbO_3$ crystal in a low repetition rate amplified laser system. By aligning our laser polarization to the ordinary polarization eigenmode and by pre-aberrating the beam to compensate for the aberration we have demonstrated that the fabrication depth and the strength of the photonic stopgap of PhCs fabricated with this method are both increased by a factor of two to three, compared with those fabricated without adaptive optics. Furthermore, we have demonstrated that an adaptive compensation scheme is required for fabrication of the highest quality PhCs. These dramatic improvements will allow for greater freedom in the fabrication of complex devices requiring the control of the propagation direction and optical activation. Furthermore, the reduced axial size of individual voxels may allow for a reduction of the lattice constant to create the functionality at wavelengths lower than 1.5 μm, provided the effect of scatting is reduced.